Chemical Engineering Journal 165 (2010) 891–901

Contents lists available at ScienceDirect

Chemical Engineering Journal

journal homepage: www.elsevier.com/locate/cej

The photochemical thermodynamic efficiency factor (PTEF) in photocatalytic reactors for air treatment

Juan Manuel Garcia Hernandez [a], Benito Serrano Rosales [b], Hugo de Lasa [a,*]

[a] Chemical Reactor Engineering Centre (CREC), Department of Chemical and Biochemical Engineering, Faculty of Engineering, University of Western Ontario, London, Ontario, Canada N6A 5B9
[b] Facultad de Ciencias Químicas, Programa de Ingeniería Química, Universidad Autónoma de Zacatecas, Mexico

ARTICLE INFO

Article history:
Received 2 March 2010
Received in revised form 18 June 2010
Accepted 25 June 2010

Keywords:
Air
Acetone
Acetaldehyde
Heterogeneous photocatalysis
Photo-CREC-Air reactor
Reactor efficiency

ABSTRACT

The photochemical thermodynamic efficiency factor (*PTEF*) and the quantum yield (*QY*) are key parameters for assessing photocatalytic degradation efficiency and photocatalytic reaction pathways in air treatment. *QYs* and *PTEFs* can be established in a Photo-CREC-Air reactor unit on the basis of the number of *OH•* consumed, the enthalpy of *OH•* formation and the radiation reaching the photocatalyst. While the *PTEF* has been considered for photocatalytic conversion of organic pollutants in water, this is the first attempt where a *PTEF* is considered in air treatment units. Efficiency calculations are performed in the present study, using the data for acetone and acetaldehyde photocatalytic degradation in air with low concentration of water. It is shown that quantum yields both for acetone and acetaldehyde supersede the value of 1 (equivalent to 100%) while *PTEFs* remain in both cases below the level of 1 as required by thermodynamic constrains. On this basis, a chain reaction mechanism can be supported for photocatalytic conversion of organic pollutants in air.

1. Introduction

Photocatalysis is the segment of catalysis, which covers the range of the reactions proceeding under the action of light. During the last decades much attention has been paid to the reactions that take place on the irradiated surface of semiconductor metal oxides and sulfides. Studies involving gas-phase heterogeneous photocatalysis are relatively few in number compared with the substantial literature on photocatalytic water treatment [1–4]. At moderate conditions (room temperature, one atmosphere pressure and with molecular oxygen as the oxidant), some semiconductors have proved to be effective photocatalysts for the thermodynamically favored conversion of many organics into CO_2 and H_2O. The number of contributions in this area is however considerably growing nowadays given the interest of potential applications to remove organic contaminants contained in air atmospheres as found in aircraft and spacecraft, office buildings and factories.

Semiconductor materials that can promote reactions in the presence of light and are not consumed in the overall reaction are referred to as photocatalysts. In order for a semiconductor to be photochemically active as a sensitizer for the photochemical reaction the redox potential of the photogenerated valence band hole must be sufficiently positive to generate *OH•* radicals, which can subsequently oxidize the organic pollutant. The redox potential of the photogenerated conductance band electron must be sufficiently negative to be able to reduce adsorbed O_2 to superoxide [5]. Among many semiconductor photocatalysts, there is a general consensus among researchers that TiO_2 is superior because of its high activity, large stability to light illumination, low price, and lack of toxicity [6,7]. The two principal polymorphs of TiO_2 are anatase and rutile which are associated with bandgap energies of 3.2 and 3.1 eV, respectively. It has been pointed out that the photo-degradation reaction rate is mainly affected by the crystalline state and textural properties, particularly, surface area and particle size of the TiO_2 powder [8]. The photocatalytic performance of TiO_2 depends not only on its bulk energy band structure, but also, to a large extent, on surface properties such as specific surface area and coverage by *OH•* groups.

The influence of water vapour on gas phase photocatalytic oxidation depends on several factors [9,10], being the morphology of the photocatalyst, the compound to be oxidized and the amount of water vapour the main ones. Ibrahim and de Lasa [11] carried out the photo-degradation of acetone and acetaldehyde in air containing 3 ppmv of water using TiO_2 in the Photo-CREC-Air Reactor. Proposed models described well the observed kinetics.

One of the most significant obstacles in the application of photocatalytic processes is their perceived energy efficiency. Therefore it is important to establish how the irradiation is being used, or how this energy efficiency varies at different operating conditions. Consequently, in photocatalytic processes, in addition to the efforts

* Corresponding author. Tel.: +1 519 661 2144; fax: +1 519 661 3498.
E-mail address: hdelasa@eng.uwo.ca (H. de Lasa).

1385-8947/$ – see front matter © 2010 Elsevier B.V. All rights reserved.
doi:10.1016/j.cej.2010.06.034

Nomenclature

A illuminated area of catalyst, m^2
A_{irr} irradiated mesh area holding the catalyst, m^2
c speed of light in vacuum, $m\,s^{-1}$
C concentration, $\mu mole\,m^{-3}$
C_i concentration of i species, $\mu mole\,m^{-3}$
C_j concentration of j species, $\mu mole\,m^{-3}$
$C_{ACETALDEHYDE,T}$ total concentration of acetaldehyde, μmole/L
$C_{ACETONE,T}$ total concentration of acetone, μ
E_{av} average energy of a photon, J
$E(\lambda)$ energy of a photon at a given wavelength, J
h Planck's constant $J\,s\,photon^{-1}$
$I(\lambda)$ intensity of light, $W\,cm^{-2}$
$k_{ACETALDEHYDE}$ reaction rate constant for acetaldehyde, $\mu mole\,m^{-3}\,min^{-1}$
$k_{ACETONE}$ reaction rate constant for acetone, $\mu mole\,m^{-3}\,min^{-1}$
k_i intrinsic kinetic constant for i species, $\mu mole\,m^{-3}\,min^{-1}$
K adsorption constant
K_i^A adsorption constant for i species, $m^3\,\mu mole^{-1}$
K_j^A adsorption constant for j species, $m^3\,\mu mole^{-1}$
$K_{ACETALDEHYDE}^A$ acetaldehyde adsorption constant, $m^3\,\mu mole^{-1}$
$K_{ACETONE}^A$ acetone adsorption constant, $m^3\,\mu mole^{-1}$
$K'_{ACETALDEHYDE}$ dimensionless acetaldehyde adsorption constant
$K'_{ACETONE}$ dimensionless acetone adsorption constant
$C_{ACETALDEHYDE,g}$ concentration of acetaldehyde in the gas phase, $\mu mole\,m^{-3}$
$C_{ACETONE,g}$ concentration of acetone in the gas phase, $\mu mole\,m^{-3}$
$N_{ACETALDEHYDE,T}$ total number of moles of acetaldehyde
$N_{ACETONE,T}$ total number of moles of acetone
$N_{ACETALDEHYDE,g}$ number of moles of acetaldehyde in the gas phase
$C_{ACETONE,g}$ number of moles of acetone in the gas phase
$N_{ACETALDEHYDE,s}$ number of moles of acetaldehyde adsorbed on the solid
$N_{ACETONE,s}$ number of moles of acetone adsorbed on the solid
$q_{ACETALDEHYDE}$ amount of acetaldehyde adsorbed, $\mu mole\,g^{-1}$
$q_{ACETONE}$ amount of acetone adsorbed, $\mu mole\,g^{-1}$
$q_{ACETALDEHYDE,max}$ maximum amount of acetaldehyde adsorbed on solid, $\mu mole\,g^{-1}$
$q_{ACETONE,max}$ maximum amount of acetone adsorbed on the solid, $\mu mole\,g^{-1}$
Q_{used} rate of irradiated energy used to form $OH^{\bullet}$ radicals, W
Q_a rate of irradiated energy absorbed in photocatalytic reactor, W
Q_r rate of irradiated energy reaching the catalyst, W
QY^*_{app} apparent quantum yield based on $OH^{\bullet}$ radical consumption
r reaction rate
$r_{ACETALDEHYDE}$ reaction rate of acetaldehyde, $\mu mole\,m^{-2}\,min^{-1}$
$r_{ACETONE}$ reaction rate of acetone, $\mu mole\,m^{-2}\,min^{-1}$
$r_{ACETALDEHYDE,g}$ rate of acetaldehyde photocatalytic degradation as observed by concentration changes in the gas phase, $\mu mole\,m^{-2}\,min^{-1}$
$r_{ACETONE,g}$ rate of acetone photocatalytic degradation as observed by concentration changes in the gas phase, $\mu mole\,m^{-2}\,min^{-1}$
$r_{OH^{\bullet},T}$ total reaction rate of formation of $OH^{\bullet}$ radical groups per unit weight of irradiated catalyst, $\mu mole\,gcat_{irr}^{-1}\,s^{-1}$
$r_{OH^{\bullet},j}$ reaction rate of $OH^{\bullet}$ radicals in reaction step j, $\mu mole\,gcat_{irr}^{-1}\,s^{-1}$
$r_{i,j}$ reaction rate of component i in reaction step j, $\mu mole\,gcat_{irr}^{-1}\,s^{-1}$
V total system volume, m^3
W weight of adsorbent material, g
W_{irr} total amount of irradiated catalyst, g

Acronyms
PTEF photochemical thermodynamic efficiency factor
QY quantum yield

Subscripts
ads adsorbed
app apparent
av average
irr irradiated
max maximum
min minimum

Greek letters
γ fraction of the adsorbed energy contributed by photons with $\lambda < 388$ nm
ν stoichiometric coefficient for the consumption of $OH^{\bullet}$ group
ν_1 stoichiometric coefficient for the consumption of model pollutant
$\nu_{ACETALDEHYDE}$ stoichiometric coefficient of acetaldehyde
$\nu_{ACETONE}$ stoichiometric coefficient of acetone
$\nu_{OH^{\bullet},j}$ stoichiometric coefficient of $OH^{\bullet}$ radical in reaction step j
$\nu_{H_2O,j}$ stoichiometric coefficient of H_2O in reaction step j
$\nu_{h,j}$ stoichiometric coefficient of component h in reaction step j
$\nu_{i,j}$ stoichiometric coefficient of component i in reaction step j
θ_{A1} $1/(k_{ACETONE}K_{ACETONE}^A)$, min
θ_{A2} $1/k_{ACETONE}$, $m^3\,min\,\mu mole^{-1}$
θ_{AA1} $1/(k_{ACETALDEHYDE}K_{ACETALDEHYDE}^A)$, min
θ_{AA2} $1/k_{ACETALDEHYDE}$, $m^3\,min\,\mu mole^{-1}$
$\eta_{OH^{\bullet}}$ fraction of photon energy to form $OH^{\bullet}$ radicals
λ radiation wavelength, nm
λ_{max} upper bound of wavelength in the range of interest, nm
λ_{min} lower bound of wavelength in the range of interest, nm
$\zeta_{ACETALDEHYDE}$ dimensionless solid phase acetaldehyde concentration
$\zeta_{ACETONE}$ dimensionless solid phase acetone concentration
$\Delta H_{OH^{\bullet}}$ enthalpy of formation of an $OH^{\bullet}$ group adsorbed on the photocatalyst, $J\,mol^{-1}$
$\Delta H^{\circ}_{f,OH^{\bullet}(g)}$ standard enthalpy of formation of $OH^{\bullet}$ radical, $J\,mole^{-1}$
$\Delta H^{\circ}_{f,H_2O(g)}$ standard enthalpy of formation of water vapor, $J\,mole^{-1}$
$\Delta H^{\circ}_{f,O_2(g)}$ standard enthalpy of formation of O_2, $J\,mole^{-1}$

directed at obtaining high active photocatalysts and at identifying best operating conditions, it is also necessary to pay special attention to the reactor design factors restricting the optimal use of the radiation.

A key tool for this analysis is the quantum efficiency; this parameter also can help in the discrimination of reaction pathways. Different definitions have been proposed in photoreactors, leading to different ways of assessing their energy performance [12–14]. Ibrahim [15] and de Lasa et al. [2] provided detailed summaries of the possible quantum yield definitions as well as their concise description. Reported definitions are based on a ratio that involves either photoconverted molecules over "absorbed photons" or photoconverted molecules over "photons entering the reactor".

Given the lack of bounds for quantum efficiency, Serrano and de Lasa [16] proposed a Photocatalytic thermodynamic efficiency factor (*PTEF*) based on thermodynamic considerations for water purification units. It was shown in this regard [17] that in Photo-CREC-Water photocatalytic reactors for water purification both quantum efficiency and *PTEF* display encouraging values that remain consistently below 1. As a result a reaction mechanism based on $OH^{\bullet}$ radical consumption is likely to rule.

It is the purpose of this study to establish similar bounds in photocatalytic reactors for air treatment and to assess potential reaction pathways on the basis of *PTEFs* and quantum yields.

2. Quantum yield and photochemical thermodynamic efficiency factor (PTEF)

The *"apparent quantum yield"* is a parameter frequently used to evaluate the photon efficiency as the ratio of pollutant molecules degraded over the number of photons entering the reactor and with enough energy to supersede the photocatalyst band gap [17]. For near-UV lamps the following definition can be adopted:

$$QY_{app} = \frac{\text{number of pollutant molecules photoconverted}}{\text{number of photons reaching the photocatalyst with } \lambda \leq 388\ \text{nm}} \quad (1)$$

This definition can be modified and established in a more phenomenological meaningful manner [17], expressing the apparent quantum yield as the ratio of the rate of $OH^{\bullet}$ radicals converted at any time during the photoconversion over the rate of photons reaching the photocatalyst as,

$$QY^{*}_{app} = \frac{\text{number of } OH^{\bullet} \text{ consumed}}{\text{number of photons reaching the photocatalyst with } \lambda \leq 388\ \text{nm}} \quad (2)$$

This above definition of the *"apparent quantum yield"* assuming the $OH^{\bullet}$ species consumed as the sole radical driving the photoconversion process is based on the stoichiometric requirements for oxidation of observable chemical species [18]. This definition assigns to the $OH^{\bullet}$ radicals the role of driving the photocatalytic reaction and can be considered a *"maximum apparent quantum yield"*.

For instance, for the "*j*" chemical reaction step, one can consider that both $OH^{\bullet}$ groups and two organic species are involved, with a different degree of oxidation. The "*i*" species ($C_nH_mO_o$) represents the species at the lower oxidation state while the "*h*" species ($C_xH_yO_z$) the one at the higher oxidation state. These two species have to comply with oxygen, carbon, and hydrogen elemental balances as needed by stoichiometric requirements. Thus, stoichiometric equations set the $OH^{\bullet}$*s* needed in every "*j*" photocatalytic step where "*i*" ($C_nH_mO_o$) species are transformed into "*h*" ($C_xH_yO_z$) species as follows,

$$\nu_{i,j}C_nH_mO_o + \nu_{OH,j}OH^{\bullet} \rightarrow \nu_{h,j}C_xH_yO_z + \nu_{H_2O,j}H_2O \quad (3)$$

with $\nu_{i,j}$ and $\nu_{h,j}$ representing the stoichiometric coefficients for $C_nH_mO_o$ and $C_xH_yO_z$, respectively for the "*j*" step with,

$$\nu_{i,j}n - \nu_{h,j}x = 0 \quad \text{(elemental carbon balance)} \quad (4a)$$

$$\nu_{i,j}m + \nu_{OH^{\bullet},j} - \nu_{h,j}y - 2\nu_{H_2O,j} = 0 \quad \text{(elemental hydrogen balance)} \quad (4b)$$

$$\nu_{i,j}o + \nu_{OH^{\bullet},j} - \nu_{h,j}z - \nu_{H_2O,j} = 0 \quad \text{(elemental oxygen balance)} \quad (4c)$$

$$\text{As a result } r_{OH^{\bullet},T} = \sum r_{OH^{\bullet},j} = \sum \frac{\nu_{OH^{\bullet},j}}{\nu_{i,j}} r_{i,j} \quad (5)$$

where $r_{OH^{\bullet},j}$ is the rate of consumption of $OH^{\bullet}$ radicals in step "*j*" of the reaction network, $r_{i,j}$ is the reaction rate of the compound "*i*" in step "*j*", and $\nu_{i,j}$ is the stoichiometric coefficient of compound "*i*" in step "*j*". One should mention that sometimes stoichiometric coefficients in Eq. (5) may be zero with this depending on the contribution of "*i*" species in a specific reaction step "*j*".

Thus, it is shown that the total rate of $OH^{\bullet}$ consumption can be calculated using an *"indirect method"* as in Eq. (5), involving the summation of the rates of every single oxidation step multiplied by the ratio of the corresponding stoichiometric coefficients as,

$$QY^{*}_{app} = \frac{-W_{irr}\sum_1^j r_{OH^{\bullet},j}}{\int_{\lambda_{min}}^{\lambda_{max}=388\,\text{nm}} RA_{irr}\lambda d\lambda/hc} = \frac{\sum_1^j \frac{\nu_{OH,j}}{\nu_{i,j}} r_{i,j}}{\int_{\lambda_{min}}^{\lambda_{max}=388\,\text{nm}} RA_{irr}\lambda d\lambda/hc} \quad (6)$$

with: $r_{OH^{\bullet},j}$ is the rate of $OH^{\bullet}$ radicals conversion in step "*j*" (mol/gcat$_{irr}$ s); $r_{i,j}$ is the rate of "*i*" pollutant molecules degraded in the step "*j*" of the photoconversion process (mol/gcat$_{irr}$·s); $\nu_{i,j}$ is the stoichiometric coefficient involved in the photoconversion of the species "*i*" in step "*j*"; *R* is the radiation intensity, W/(cm^2 nm); $A_{irr}$is the total area of irradiated photocatalyst-impregnated mesh, 510 cm^2; *h* is the Planck's constant, 6.63×10^{-34} J s; *c* is the speed of light in vacuum, 3×10^{10} cm/s; λ_{min} is the lower wavelength of the spectrum in the range of interest, 300 nm; λ_{max} is the higher wavelength of the spectrum in the range of interest, 388 nm.

The photochemical thermodynamic efficiency factor (*PTEF*) for photocatalytic air treatment units is a parameter relating the energy utilized for the $OH^{\bullet}$ radical formation over the irradiated energy on the photocatalyst. This definition has to be modified including a γ parameter which represents the fraction of the photon energy with a wavelength smaller than the one needed for superseding the semiconductor band gap.

$$PTEF_{app} = \frac{Q_{used}}{Q_{irr}\gamma} = \frac{-r_{OH^{\bullet},T}\Delta H_{OH^{\bullet}} W_{irr}}{Q_{irr}\gamma} \quad (7)$$

with $r_{OH^{\bullet},T}$ being in mol min^{-1}gcat$_{irr}^{-1}$, W_{irr} in gcat$_{irr}$, $\Delta H_{OH^{\bullet}}$ in J mol^{-1}, Q_{irr} in J min^{-1} and γ without units.

The *PTEF* can be also portrayed as the product of *QY* and $\eta_{OH^{\bullet}}$ [17], with *QY* accounting for the fraction of photons absorbed by the photocatalyst leading to the formation of $OH^{\bullet}$ radicals (quantum yield):

$$PTEF_{app} = QY_{app}\eta_{OH^{\bullet}} \quad (8)$$

where $\eta_{OH^{\bullet}}$ is the fraction of photon energy used in forming an $OH^{\bullet}$ radical, given by

$$\eta_{OH^{\bullet}} = \frac{\Delta H_{OH^{\bullet}}}{E_{av}} \quad (9)$$

with $\Delta H_{OH^{\bullet}}$ being the enthalpy of formation of an $OH^{\bullet}$ group (J mol^{-1}) and E_{av} the average energy of a photon (J) (Appendix I).

As it is shown in this section, one can expand the *PTEF* definition to photocatalytic reactors for air treatment introducing a judiciously selected photocatalytic reaction network and kinetics as well as relevant thermodynamic and irradiation parameters.

3. Reaction enthalpy for the formation of $OH^{\bullet}$ radicals in photocatalytic reactors for air treatment

The formation enthalpy of $OH^{\bullet}$ is a critical parameter for the calculation of *PTEF* in photocatalytic reactors as shown in Section 2.

According to stoichiometric requirements $OH^{\bullet}$ radicals can be formed via the overall equation (Appendix II)

$$H_2O_{(g)} + \tfrac{1}{2}O_{2(g)} \rightarrow 2OH_{ads}{}^{\bullet} \quad (10)$$

Enthalpy evaluations in Eq. (10) can consider one "likely" path for evolving reactant species (water vapor and oxygen) forming adsorbed $OH^{\bullet}$ radicals (products). This hypothetical reaction path gives the correct numerical result, given this calculation involves enthalpies (state functions).

The proposed "likely" path for thermodynamic evaluations considers that the reaction takes place as follows: (a) oxygen gas is adsorbed on the photocatalyst surface, (b) water vapor is adsorbed on the photocatalyst surface, (c) adsorbed $OH^{\bullet}$ species are formed via reaction of adsorbed oxygen and water species. It is in this adsorbed state where $OH^{\bullet}$ radicals are assumed to react with organic molecules forming intermediates first and CO_2 later when complete mineralization is reached.

Thus for,

$$O_2(g) + S \rightarrow O_{2ads} \quad \Delta H_1 = \Delta H^{\circ}_{f,O_2ads} - \Delta H^{\circ}_{f,O_2(g)} \quad (11)$$

$$H_2O(g) + S \rightarrow H_2O_{ads} \quad \Delta H_2 = \Delta H^{\circ}_{f,H_2Oads} - \Delta H^{\circ}_{f,H_2O(g)} \quad (12)$$

$$O_{2ads} + 2H_2O_{ads} + S \rightarrow 4OH_{ads}{}^{\bullet}$$

$$\Delta H_3 = \Delta H^{\circ}_{f,OH^{\bullet}ads} - \frac{1}{2}\Delta H^{\circ}_{f,H_2Oads} - \frac{1}{4}\Delta H^{\circ}_{f,O_2ads} \quad (13)$$

The algebraic addition of these three steps leads to the following:

$$O_2(g) + 2H_2O(g) + 4S \rightarrow 4OH_{ads}{}^{\bullet};$$

$$\Delta H_{OH^{\bullet}} = \left[\Delta H_3 + \frac{1}{2}\Delta H_2 + \frac{1}{4}\Delta H_1\right] = \Delta H_3 = \Delta H^{\circ}_{f,OH^{\bullet}ads} - \frac{1}{2}\Delta H^{\circ}_{f,H_2O(g)} - \frac{1}{4}\Delta H^{\circ}_{f,O_2(g)} \quad (14)$$

It is worth noting that the adsorption mechanism that possibly prevails in photocatalytic processes is the one of chemisorptions and as a result a good estimation of the heat of adsorption is via the heat of condensation [19,20]. Using the heat of formation data reported by Wagman et al. [21] and Kyle [22], the adsorption enthalpy of $OH^{\bullet}$ radical species results as,

$$\Delta H^{\circ}_{f,OH^{\bullet}ads} = 38,950\,\text{J/mol} - (-86,490\,\text{J/mol}) = 125,440\,\text{J/mol} \quad (15)$$

Then the enthalpy of formation of the $OH^{\bullet}$ groups adsorbed on the photocatalyst surface starting from both H_2O and O_2 species both in the gas phase is,

$$\Delta H_{OH^{\bullet}} = 125,440\,\text{J/mol} - \frac{1}{2}(23181\,\text{J/mol}) \quad (16)$$

$$\Delta H_{OH^{\bullet}} = 4531\,\frac{J}{\text{mol of } OH^{\bullet}} \quad (17)$$

While a similar analysis was developed by Serrano et al. [17] for a photocatalytic reactor for water purification, the enthalpy of adsorbed $OH^{\bullet}$ radical for air treatment photocatalytic reactor is here reported. This enthalpy is noticeably and justifiable smaller than the 98,300 J/mol enthalpy reported by Serrano et al. [17]. This creates a different and interesting scenario in terms of energy efficiencies in photocatalytic reactors for air treatment versus the ones for water decontamination.

Since the enthalpy required to produce an adsorbed $OH^{\bullet}$ group is 4531 J/mol of $OH^{\bullet}$, the fraction of photon energy used to form an $OH^{\bullet}$ radical is

$$\eta_{OH^{\bullet}} = \frac{\Delta H_{OH^{\bullet}}}{E_{av}} = \frac{4531(\text{J/mol of } OH^{\bullet})}{343,913(\text{J/mol of photon})} = 0.0131748\,\frac{\text{mol of photon}}{\text{mol of } OH^{\bullet}} \quad (18)$$

4. Experimental setup and methods

The present manuscript uses the kinetic data obtained in a laboratory scale version of Photo-CREC-Air using immobilized non-porous 35–36 m^2/g Degussa P25 particles and porous 300 m^2/g Hombikat UV-100 particles [23]. The Photo-CREC-Air unit was operated in batch mode with a given amount of model pollutant injected in a set volume of air; the model pollutant was vaporized almost instantaneously and mixed completely with the air stream.

4.1. Photo-CREC-Air reactor

The main body of the Photo-CREC-Air reactor consists of a closed-loop system with 14.7 L of capacity and is made of zinc-plated pipes connected with aluminized-steel 90° elbows and a stainless steel Venturi section. There are eight Pen-Ray 1-watt lamps symmetrically placed around the reaction section, which is constituted by a basket supporting fiberglass mesh and immobilized TiO_2. The radiation penetrates through windows cut out of acrylic sheets in a divergent section of the Venturi. The photo-CREC–air batch reactor unit with auxiliary components is described in Fig. 1 [11].

The description of the mesh and the techniques implemented to impregnate the photocatalyst were reported elsewhere by Ibrahim and de Lasa [23]. It was stated that an increase in the photo-conversion rate with catalyst loading is linked to an increase in the catalyst irradiated area an in turn to a higher photon absorption rate. Given the fact that the increase in the TiO_2 loading produced a thicker catalyst layer, this increase of the TiO_2 yielded higher rates of UV photon absorption and therefore higher photo-conversion rates. Even more, a critical photocatalyst thickness was reported; surpassing this critical thickness little enhancement of photon absorption and photo-conversion rate was detected. This critical layer thickness was estimated to be in the 5.4 μm range; being in agreement with the information reported by other authors with respect to the UV–light absorption within TiO_2 catalysts [24,25].

Air exiting the blower enters the Venturi divergent section, flows through the Venturi throat and contacts the TiO_2-impregnated mesh (Fig. 2(c)). The fluid flow pattern in the Photo-CREC-Air has been assessed and characterized by our research team [26]. The optimum loadings of TiO_2 were reported by Ibrahim and the Lasa [23], being 8.0–8.8 wt.% for Degussa P25 and 3.6–4.8 for Hombikat UV-100. Eight Pen-Ray Mercury UV-lamps, with a power output of 1213 μW cm^{-2} at 20 mA (AC) and a principal radiation wavelength of 365 nm, mounted outside of the Venturi divergent section (Fig. 2(a)) and housed inside parabolic reflectors irradiate the TiO_2-impregnated mesh. The parabolic reflectors are designed so that the irradiation focal point is placed at a semi-infinite distance from the source, thereby improving the incidence efficiency Ibrahim [15].

Ibrahim and de Lasa [14] reported the experimental procedure followed to carry out the experimental runs: (a) the system was flushed with zero 0.1 grade dry air containing 3 ppmv of H_2O, (b) the pressure regulators were closed and the fan was turned on, (c) a liquid sample of model pollutant was injected and a 60 min period was allowed for system stabilization. Pollutants were injected into the reactor via the injection port and using a CR-700 syringe, (d) once the adsorption equilibrium reached ("dark reaction"), lamps

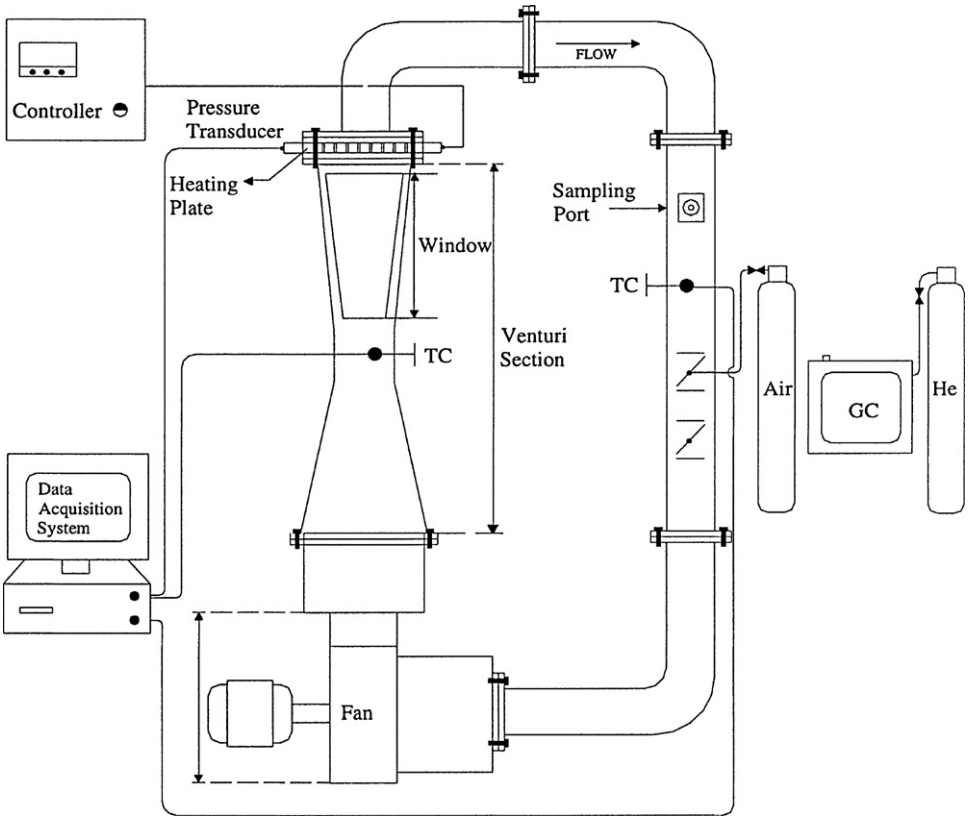

Fig. 1. Schematic diagram of the Photo-CREC-Air reactor [11].

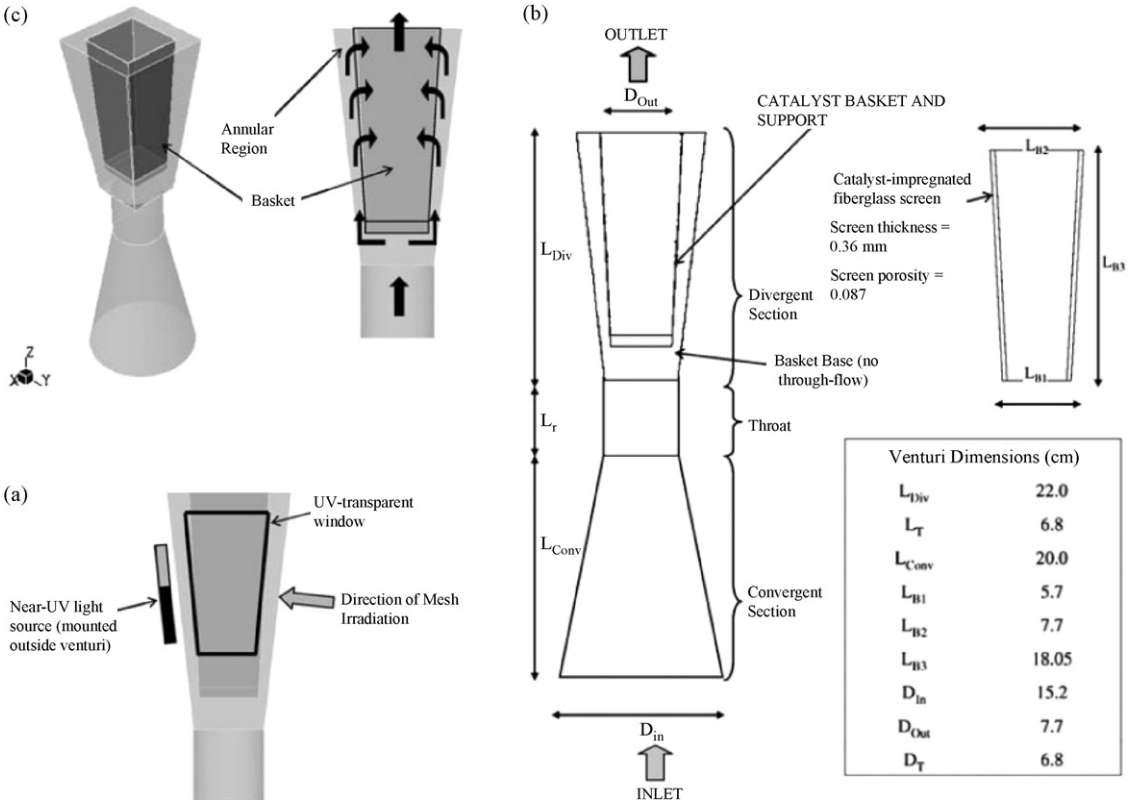

Fig. 2. Photo-CREC–air Venturi section: (a) mesh irradiation by externally mounted near-UV lamps. (b) Venturi and basket dimensions. (c) Venturi divergent section and Venturi isometric view [26].

were turned on and the reaction was allowed to proceed, (e) gas samples were taken periodically, (f) at the end of each run, lamps were turned off and the reactor was flushed with dry air, (g) Following this, the mesh was replaced after very experiment; following this the reactor was ready for a new run.

Acetone and acetaldehyde (Both supplied by Caledon Laboratories Ltd., 99% purity) were used as model pollutants during the aforementioned study. Different amounts of liquid pollutant were injected into the 14.7 L reactor to attain the desired gas phase concentrations: 40, 50 and 60 μL for the case of acetone and 30, 40 and 50 μL for acetaldehyde. The reactor operates with a gas chromatograph HP 5890 equipped with an HP3393A integrator, a TCD and a Poropak Q packed column allowing the identification and quantification of all the present chemical species.

Species balances in the Photo-CREC-Air unit can be established given the various gas mixing, catalyst dispersion on the mesh and mesh irradiation, applicable assumptions via the following equation:

$$V\frac{dC}{dt} = rA_{irr} \tag{19}$$

where: V is the total hold up of the gas, m^3; C is the model pollutant concentration, $\mu mol/m^3$; r is the rate of photo conversion of the model pollutant under study, $\mu mol/(m^2\,min)$; A_{irr} is the irradiated area of catalyst, m^2.

5. Stoichiometric equations and photoreaction rates

5.1. Acetone photocatalytic degradation stoichiometry

Assuming acetone photocatalytic degradation is the result of the $OH^\bullet$ group consumption rate only, the following stoichiometry can be proposed:

$$C_3H_6O + 16OH^\bullet \rightarrow 3CO_2 + 11H_2O \tag{20}$$

This stoichiometry applies given no intermediate species were detected as documented by Ibrahim and de Lasa [11].

As a result the following relationships can be considered,

$$\frac{r_{ACETONE}}{\nu_{ACETONE}} = \frac{r_{OH^\bullet}}{\nu_{OH^\bullet}} \quad \text{and} \quad r_{OH^\bullet} = \frac{\nu_{OH^\bullet}}{\nu_{ACETONE}} r_{ACETONE} \tag{21}$$

where: $\nu_{ACETONE}$ is the stoichiometric coefficient for acetone; $\nu_{OH^\bullet}$ is the stoichiometric coefficient for $OH^\bullet$.

5.2. Acetaldehyde photocatalytic degradation stoichiometry

In a similar manner and as it is considered for acetone, the following stoichiometry can be adopted for acetaldehyde degradation with the assumption that the only radical species driving the photocatalytic degradation are $OH^\bullet$ radicals:

$$C_2H_4O + 10OH^\bullet \rightarrow 2CO_2 + 7H_2O \tag{22}$$

This stoichiometry also assumes that there are no intermediates and as a result the rate of photoconversion of acetaldehyde and the $OH^\bullet$ group consumption rate can be related as follows:

$$\frac{r_{ACETALDEYDE}}{\nu_{ACETALDEHYDE}} = \frac{r_{OH^\bullet}}{\nu_{OH^\bullet}} \quad \text{and} \quad r_{OH^\bullet} = \frac{\nu_{OH^\bullet}}{\nu_{ACETONE}} r_{ACETONE} \tag{23}$$

where: $\nu_{ACETALDEHYDE}$ is the stoichiometric coefficient for acetaldehyde; $\nu_{OH^\bullet}$ is the stoichiometric coefficient for $OH^\bullet$.

6. Photocatalytic modeling

The photocatalytic reaction kinetics can be modeled with a Langmuir–Hinshelwood expression,

$$r = \frac{-k^* I^\alpha KC}{1 + KC + \sum K_i C_i} \tag{24}$$

with $\alpha = 1$, K is the equilibrium adsorption constant for the model pollutant and the term $\sum K_i C_i$ represents the combined effect of all adsorbed intermediate species.

This model was implemented by Ibrahim [15] and Ibrahim and de Lasa [14] to approach the kinetics of photoconversion of acetone and acetaldehyde with TiO_2 as a catalyst. This kinetics was proven adequate to describe the observed changes of the chemical species concentrations in the gas phase [11].

In order to represent the observed photocatalytic degradation kinetics the following assumption were considered: (a) the gas phase is near-UV transparent with light absorption, scattering and reflection all being negligible; (b) the mixing in the Photo-CREC-Air reactor is intense, given the high air recirculation. Gas phase concentrations of all species can be considered uniform at a given time; (c) the windows in the reaction section are free of deposited particles and the adsorption of reactants on the reactor wall materials can be neglected; (d) the mesh supporting the TiO_2 is constantly irradiated by the near-UV lamps with an intensity of light that does not change significantly during the experiments; (e) the contribution of the thermal reactions to the photoconversion process is insignificant.

6.1. Acetone photocatalytic degradation modeling

It is as well known that the amount of acetone remaining in the fluid phase is the result of adsorption and photoconversion processes. The mole balance for acetone is

$$N_{ACETONE,T} = N_{ACETONE,g} + N_{ACETONE,s} \tag{25}$$

where $N_{ACETONE,T}$ is the total number of moles of acetone, $N_{ACETONE,g}$ is the number of moles of acetone in the gas phase and $N_{ACETONE,s}$ is the number of moles adsorbed on the solid.

Dividing various term of Eq. (25) by the total system volume V it results,

$$C_{ACETONE,T} = C_{ACETONE,g} + \frac{N_{ACETONE,s}}{V} \tag{26}$$

where $C_{ACETONE,T}$ is the total concentration ($\mu mol/m^3$), $C_{ACETONE,g}$ is the number of moles of acetone in the gas phase ($\mu mol/m^3$) and V is the total system volume (m^3).

If during the photocatalytic process the adsorption equilibrium is reached at all times, the amount of acetone is given as,

$$N_{ACETONE,s} = q_{ACETONE} W = \zeta_{ACETONE} W q_{ACETONE,\max} \tag{27}$$

with

$$\zeta_{ACETONE} = \frac{q_{ACETONE}}{q_{ACETONE,\max}} \tag{28}$$

with $q_{ACETONE}$ being the specific amount of acetone adsorbed ($\mu mol/g$), $q_{ACETONE,\max}$ the maximum amount of acetone adsorbed ($\mu mol/g$) and W the total weight of the adsorbent substrate (g).

Furthermore, if the value of $\zeta_{ACETONE}$ can be related to the acetone concentration in the gas phase through a pseudo-equilibrium constant evaluated at one point of the adsorption equilibrium isotherm

$$\zeta_{ACETONE} = K^A_{ACETONE} C_{ACETONE} \tag{29}$$

Thus, the total concentration of acetone can be defined as

$$C_{ACETONE,T} = C_{ACETONE,g}\left(1 + K'_{ACETONE}\right) \tag{30}$$

Table 1
Parameters for acetone modeling [15].

Catalyst	$\theta_{A1} \times 0.1$	$\theta_{A2} \times 1000$
Degussa P25	10.77 ± 0.47	4.88 ± 0.19
Hombikat UV-100	4.06 ± 0.62	7.79 ± 0.29

where the dimensionless adsorption constant is given by

$$K'_{ACETONE} = \frac{K^A_{ACETONE} W q_{ACETONE,\max}}{V} \quad (31)$$

As a result a total reaction rate for acetone photocatalytic degradation with a reaction rate involving the observed chemical species concentration changes in the gas phase can be obtained considering the derivative of Eq. (30)

$$r_{ACETONE,T} = r_{ACETONE,g}(1 + K'_{ACETONE}) \quad (32)$$

where $r_{ACETONE,T}$ is the total reaction rate (μmol/(m^2 min)) and $r_{ACETONE,g}$ the reaction rate involving the observed chemical species concentration changes in the gas phase (μmol/(m^2 min)).

Even more given acetone was the only detectable species and given the rate of consumption for *i* species follows a Langmuir–Hinshelwood model, as described in Eq. (24), thus

$$r_{ACETONE,g} = \frac{dC_{ACETONE,g}}{dt}\frac{V}{A_{irr}} = -\frac{k_{ACETONE}K^A_{ACETONE}C_{ACETONE,g}}{1 + K^A_{ACETONE}C_{ACETONE.g}}\frac{V}{A_{irr}} \quad (33)$$

This expression can also be expressed as,

$$r_{ACETONE,g} = -\frac{C_{ACETONE,g}}{\theta_{A1} + \theta_{A2}C_{ACETONE.g}}\frac{V}{A_{irr}} \quad (34)$$

where: $r_{ACETONE,g}$ is the rate of acetone photocatalytic degradation as assessed by changes in the gas phase concentrations, μmol/(m^2·min); $C_{ACETONE,g}$ is the acetone concentration in the gas phase, μmol/m^3; A_{irr} is the irradiated mesh area holding the catalyst, m^2; $K^A_{ACETONE}$ is the acetone adsorption constant, m^3/μmol; $k_{ACETONE}$ is the reaction rate constant, μmol/(m^3 min); $\theta_{A1} = 1/(k_{ACETONE}K^A_{ACETONE})$, min; $\theta_{A2} = 1/k_{ACETONE}$, m^3 min/μmol.

Ibrahim [15] reported values of θ_{A1} and θ_{A2} for two different catalysts acting used in the photoconversion of acetone. These values are shown in Table 1.

$K'_{ACETONE}$ was evaluated for both catalysts Degussa P25 and Hombikat UV-100 to be 0.06 and 0.08, respectively.

Results of data fitting with Eq. (34) are reported in Figs. 3 and 4 for the Hombikat UV-100 and Degussa P25, respectively.

6.2. Acetaldehyde photocatalytic degradation modeling

Using a similar kinetic modeling procedure as in Section 6.1, it is possible to obtain the following expression for the acetaldehyde reaction degradation rate.

$$r_{ACETALDEHYDE,g} = \frac{dC_{ACETALDEHYDE,g}}{dt}\frac{V}{A_{irr}} = -\frac{k_{ACETONE}K^A C_{ACETALDEHYDE,g}}{1 + K^A C_{ACETALDEHYDE.g}}\frac{V}{A_{irr}} \quad (35)$$

This rate expression can be rewritten as

$$r_{ACETALDEHYDE,g} = -\frac{C_{ACETALDEHYDE,g}}{\theta_{AA} + \theta_{AA2}C_{ACETALDEHYDE.g}}\frac{V}{A_{irr}} \quad (36)$$

where: $r_{ACETALDEHYDE,g}$ is the rate of acetaldehyde photocatalytic degradation as assessed by changes in the gas phase concentrations, μmol/(m^2 min); $C_{ACETALDEHYDE,g}$ = acetaldehyde concentration in the gas phase, μmol/m^3; A_{irr} = illuminated mesh area, m^2; $K^A_{ACETALDEHYDE}$ is the acetaldehyde adsorption constant, m^3/μmole; $k_{ACETALDEHYDE}$ = reaction rate constant, μmol/(m^3 min); $\theta_{AA1} = 1/(k_{ACETALDEHYDE}K^A_{ACETALDEHYDE})$, min; $\theta_{AA2} = 1/k_{ACETALDEHYDE}$, m^3 min/μmol.

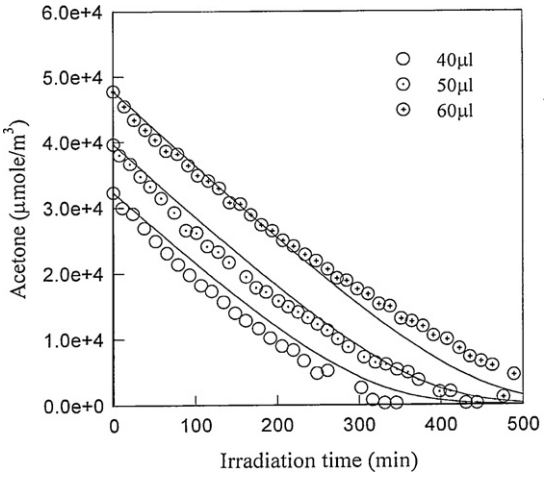

Fig. 3. Changes of acetone concentrations with reaction time using Hombikat UV-100 (full line represents model predictions) [11].

Table 2
Parameters for acetaldehyde modeling [15].

Catalyst	$\theta_{AA1} \times 0.1$	$\theta_{AA2} \times 10{,}000$
Degussa P25	5.10 ± 0.45	3.62 ± 1.55
Hombikat UV-100	1.99 ± 0.218	6.87 ± 0.89

The values of θ_{AA1} and θ_{AA2} for two different commercial catalysts acting in the photo conversion of acetaldehyde have been reported by Ibrahim [15]. These values are shown in Table 2.

$K'_{ACETALDEHYDE}$ was evaluated for both Degussa P25 and Hombikat UV-100 to be 0.07 and 0.13, respectively.

The data fitting with Eq. (36) is reported in Figs. 5 and 6 for Hombikat UV-100 and Degussa P25, respectively.

7. Results and discussion

As a result, one can conclude that the proposed kinetics [11] based in a Langmuir–Hinshelwood equation, which considers a

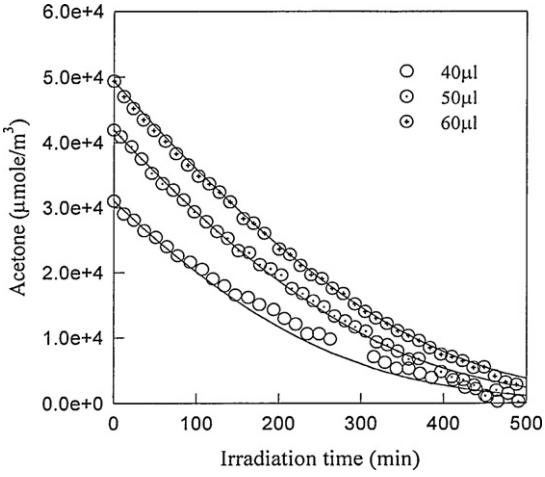

Fig. 4. Changes of acetone concentrations with reaction time using Degussa P25 (full line represents model predictions) [11].

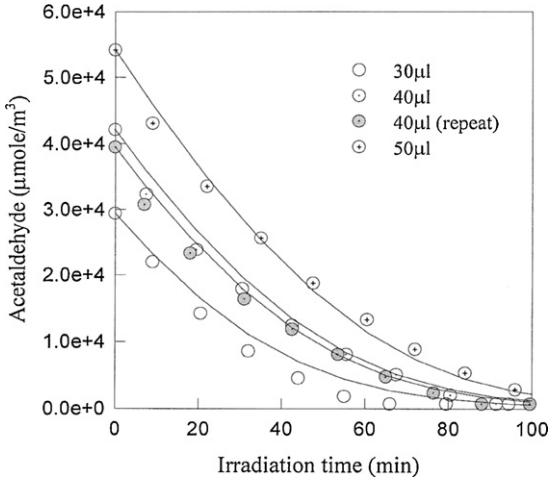

Fig. 5. Changes of acetaldehyde concentrations with reaction time using Hombikat UV-100 (full line represents model predictions) [11].

monolayer of adsorbed pollutants, is satisfactory to describe the observed photocatalytic degradation for both acetone [27–30] and acetaldehyde [31,32]. Despite the fact that intermediates have been reported for both compounds [29,30,33–36], these intermediates were not detected in the Photo-CREC-Air reactor. This result is attributed to the high photoconversion efficiency reached in Photo-CREC-Air units.

Once the kinetics of the photocatalytic degradation is established, the quantum yields and the *PTEF* can be calculated using Eqs. (6) and (8), respectively. Results for the photocatalytic degradation of acetone are reported in Figs. 7 and 8 for Hombikat UV-100 and Figs. 9 and 10 for Degussa P25. One should stress that these quantum yields and *PTEF*s are based on the more phenomenologically sound accounting of the $OH^{\bullet}$ groups consumed in the photocatalytic degradation reaction. It is also important to appreciate that the calculated efficiencies only represent higher limits for $OH^{\bullet}$ based efficiencies given that they are based on photon energy reaching the mesh-catalyst with enough energy to supersede the semiconductor bandgap [17].

From these figures it is possible to see that energy efficiencies decrease progressively with pollutant concentration, with a common pattern being established: there is a higher $OH^{\bullet}$ utilization at the higher acetone concentrations of the initial steps of photocatalytic degradation.

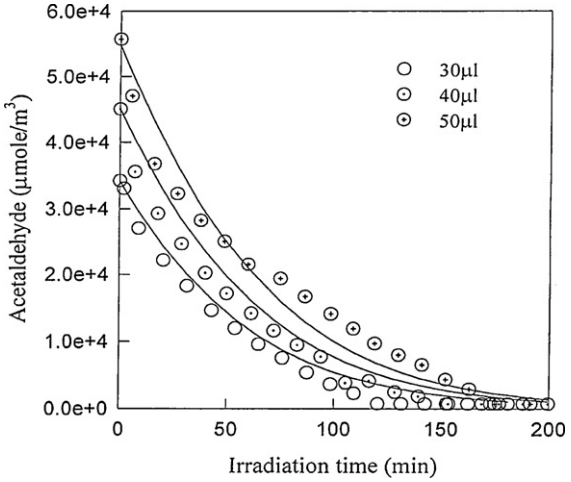

Fig. 6. Changes of acetaldehyde concentrations with reaction time using Degussa P25 (full line represents model predictions) [11].

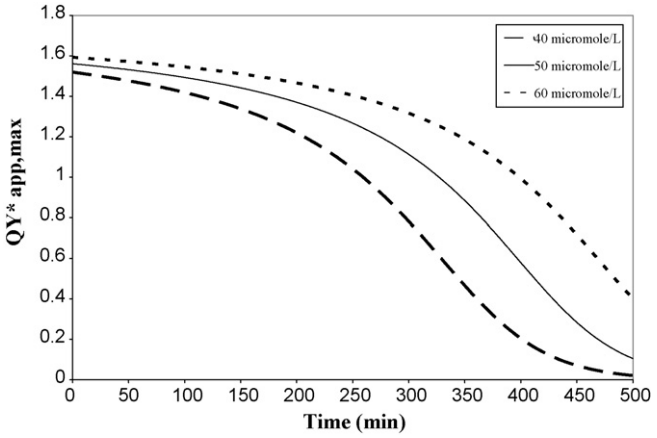

Fig. 7. $QY^{*}_{app,\max}$ for acetone using parameters from Table 1 and Fig. 3 (Hombikat UV-100). Three initial concentrations in μmole/L: 40, 50, 60 μM.

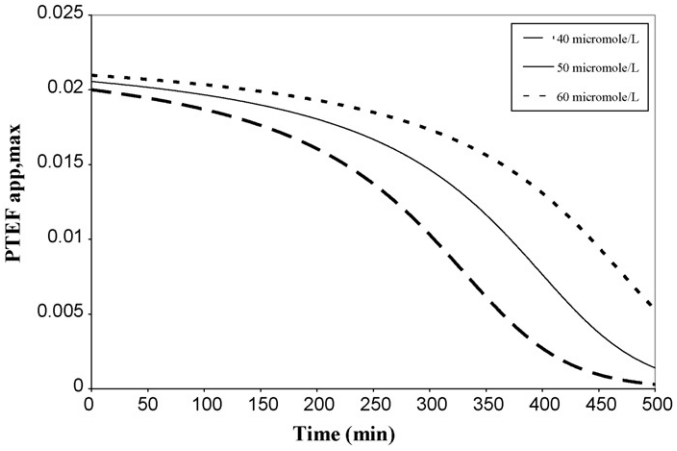

Fig. 8. $PTEF_{app,max}$ for acetone based on Table 1 and Fig. 3 (Hombikat UV-100). Three initial concentrations in μmole/L: 40, 50, 60 μM.

On the basis of the above, it is noticeably that quantum yields for acetone photocatalytic degradation are, during most of the irradiation period, in excess to the possible theoretical maximum of 133% (refer to Appendix II).

More specifically quantum yields fall in the 1.5–1.6 range (equivalent to 150–160%) for Hombikat UV-100 and 1.65–1.95

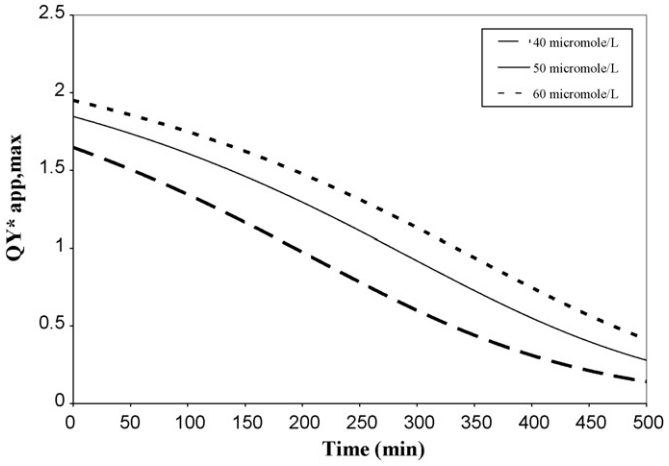

Fig. 9. $QY^{*}_{app,\max}$ for acetone using parameters from Table 1 and Fig. 4 (Degussa P25). Three initial concentrations in μmole/L: 40, 50, 60 μM.

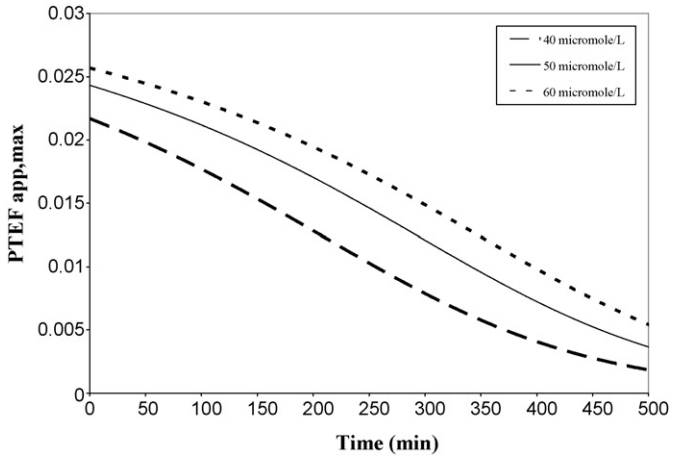

Fig. 10. $PTEF_{app,max}$ for acetone based on Table 1 and Fig. 4 (Degussa P25). Three initial concentrations in μmole/L: 40, 50, 60 μM.

range (equivalent to 165–195%) for Degussa P25 at initial irradiation conditions. However, it can also be noticed that the corresponding *PTEF*s remain in the 0.02–0.021 (2.0–2.1%) range for Hombikat UV-100 and 0.0215–0.025 (2.15–2.5%) for Degussa P25.

Thus, in spite of achieving in Photo-CREC-Air the *PTEF*s consistently below 1, the quantum yields supersede the value of 1; such as the following applies:

$$PTEF_{app,ACETONE} \leq 1 \; with \; QY^{*}_{app,\max,ACETONE} \geq 1$$

Furthermore, the quantum yields and *PTEF*s obtained during the photocatalytic degradation of acetaldehyde at three different initial concentrations using Hombikat UV-100 and Degussa P25 are reported in Figs. 11–14. The quantum yields and *PTEF*s are calculated again assuming the $OH^{\bullet}$ groups consumed are the only ones driving the photocatalytic degradation.

One can notice reviewing Figs. 11–14 that during initial irradiation the quantum yields, obtained for the photocatalytic degradation of acetaldehyde based on the consumed $OH^{\bullet}$ groups, surpass again the value of 1. These quantum yields are in the 6.3–8.15 range (equivalent to 630–815%) for Hombikat UV-100 and in the 4.6–6.7 (equivalent to 460–670%) for Degussa P25. The *PTEF*s efficiencies remain however, in the 0.08–0.10 (8–10%) and 0.06–0.087 levels (6–8.7%) for Hombikat UV-100 and Degussa P25, respectively.

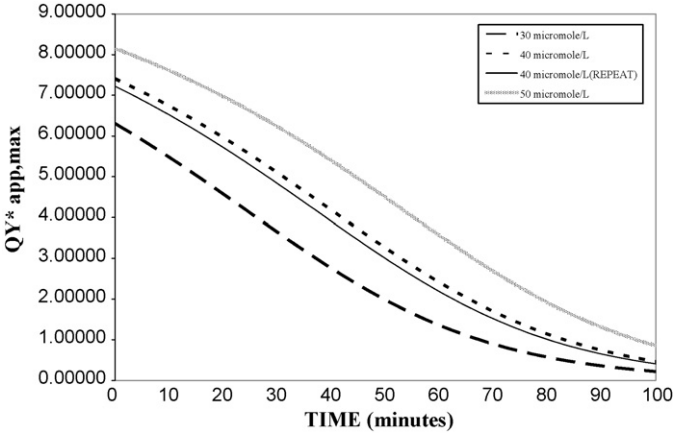

Fig. 11. $QY^{*}_{app,\max}$ for acetaldehyde based on Table 2 and Fig. 5 (Hombikat UV-100). Three initial concentrations in μmole/L: 30, 40, 40, 50 μM.

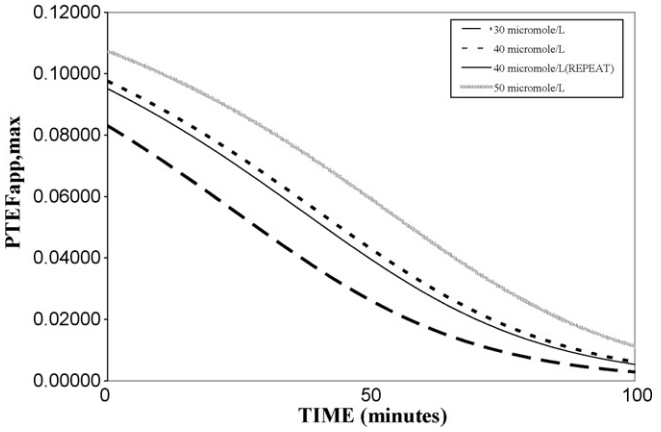

Fig. 12. $PTEF_{app,max}$ for acetaldehyde based on Table 2 and Fig. 5 (Hombikat UV-100). Three initial concentrations in μmole/L: 30, 40, 40, 50 μM.

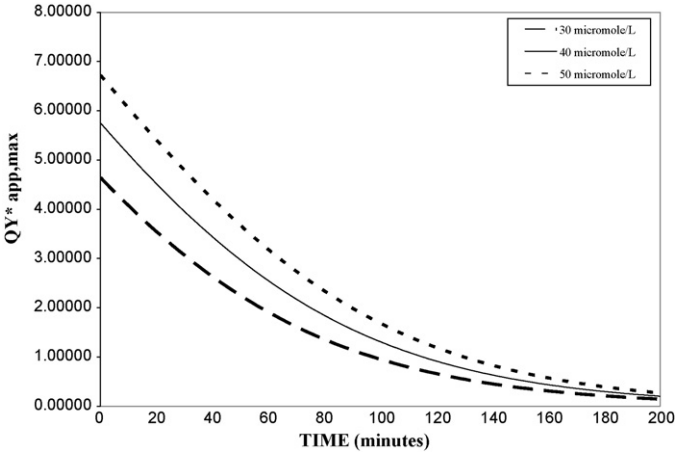

Fig. 13. $QY^{*}_{app,\max}$ for acetaldehyde based on Table 2 and Fig. 6 (Degussa P25). Three initial concentrations in μmole/L: 30, 40, 50 μM.

Thus, a similar condition is found for acetaldehyde photocatalytic degradation as in the case for acetone, with

$$PTEF_{app,ACETALDEHYDE} \leq 1 \text{ with } QY^{*}_{app,\max,ACETALDEHYDE} \geq 1.$$

It is valuable to see that in spite of finding *PTEF* values in all cases of the present study, remaining below the limit of 1 and satisfying

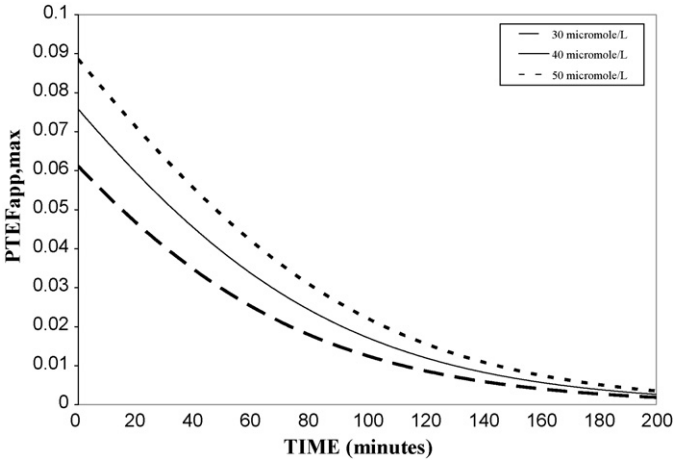

Fig. 14. $PTEF_{app,max}$ for acetaldehyde based on Table 2 and Fig. 6 (Degussa P25). Three initial concentrations in μmole/L: 30, 40, 50 μM.

in this respect thermodynamic constrains, *QYs* are in excess to 1 (equivalent to 100%),

One should also notice that the high values of *QY* reported in this study are consistent with *QYs* reported in the technical literature based on both photoconverted pollutant molecules [37–39] and formed carbon dioxide molecules [14,15].

These high *QYs*, exceeding the theoretical level of 1.33 (refer to Appendix II), can be explained via a free radical chain reaction mechanism involving other radical species such as peroxy radicals contributing to various oxidation steps and not requiring photons or *OH•* radicals to proceed [31,33]. Thus, the results of this study support consistently for both acetone and acetaldehyde photocatalytic degradation via a chain reaction pathway with photons or/and *OH•* radicals required for initiation only.

8. Conclusions

The following conclusions can be drawn from the obtained results:

a) The Photo-CREC-Air reactors display a high photocatalytic degradation of air pollutants as well as high irradiated energy efficiencies. These high energy utilization efficiencies demonstrate the suitability of Photo-CREC-Air unit designs having a well-dispersed immobilized catalyst, controlled air flow and uniform photocatalyst irradiation.
b) The photochemical thermodynamic efficiency factor (*PTEF*) is a valuable parameter together with quantum efficiencies to assess the performance of photocatalytic reactors and the reaction pathways in photocatalytic air treatment.
c) The *PTEFs* for acetone and acetaldehyde model pollutants in Photo-CREC-Air reactors using Hombikat UV-100 and Degussa P25 remain in all cases below the limit of 1 (equivalent to 100%) complying in all cases with thermodynamic constrains.
d) *QYs* however in Photo-CREC-Air units supersede in many cases the level of 1.33 (equivalent to 133%). These *QYs* could only be justified by considering a radical chain driven mechanism involving other than *OH•* radical species.

Appendix A.

A.1. Calculation of the average photon energy and the fraction of Q_{irr} with a wavelength smaller than 388 nm

The average photon energy (E_{av}) emitted by a near-UV lamp and able to activate the TiO_2 and be calculated from the irradiation spectrum which is established using a spectro-photo radiometer

$$E_{av} = \frac{\int_{\lambda_{min}}^{\lambda_{max}} I(\lambda)E(\lambda)d\lambda}{\int_{\lambda_{min}}^{\lambda_{max}} I(\lambda)d\lambda} \quad (A1.1)$$

where: $I(\lambda)$ is the intensity of light, W/cm^2; $E(\lambda)$ is the energy of a photon at a given wavelength, J.

The upper integration limit λ_{max} has a value of 388 nm wavelength, which is the highest wavelength with enough energy to supersede the catalyst (TiO_2) band gap.

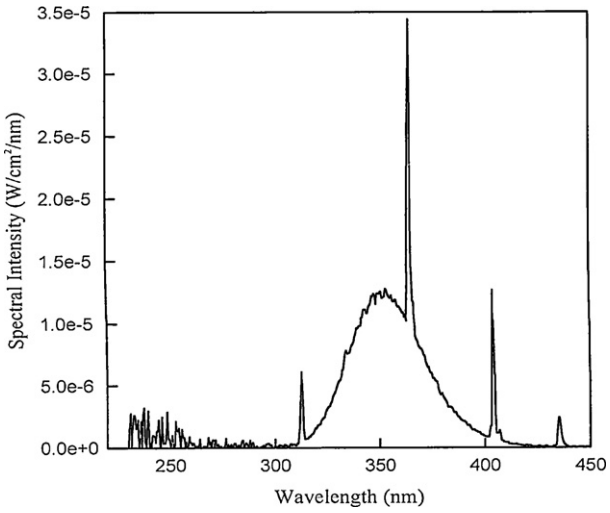

Fig. A1. Spectral intensity for a new Pen-Ray lamp as measured by the Sola Scope 2000 spectroradiometer reporting the fraction of the total energy involved in the average photon energy calculation.

Ibrahim [15] reported the spectral chart of the lamp used during the photoconversion of acetone and acetaldehyde as characterized with the Sola Scope 2000 spectroradiometer; the measurements were performed every 0.5 nm for the 300–390 nm range at different locations, confirming uniform intensity distribution of photons reaching the glass fiber mesh holding the TiO_2 loadings. Fig. A1 shows this chart.

If it is considered $E(\lambda) = (hc/\lambda)$, where h is the Planck's constant and c is the speed of light,

$$E_{av} = \frac{hc\int_{\lambda_{min}}^{\lambda_{max}} I(\lambda)(d\lambda/\lambda)}{\int_{\lambda_{min}}^{\lambda_{max}} I(\lambda)d\lambda} \quad (A1.2)$$

Thus,

$$E_{av} = \frac{hc\int_{\lambda_{min}}^{\lambda_{max}=388\,nm} I(\lambda)(d\lambda/\lambda)}{\int_{\lambda_{min}}^{\lambda_{max}=388\,nm} I(\lambda)d\lambda} = E_{av} = \frac{(6.63\times10^{-34}\,J\,s/photon)(3\times10^{8}\,m/s)}{3.48\times10^{-7}\,m} = 5.71\times10^{-19}\,(J/photon) \quad (A1.3)$$

$$E_{av} = (5.71\times10^{-19}\,J/photon)(6.023\times10^{23}\,(photon/mol\ photon)) = 343,913\,J/(mol\,photon)$$

Furthermore using the same spectrum as reported in Fig. A1 one can calculate the fraction of irradiated energy with a wavelength smaller than 388 nm as follows:

$$\gamma = \frac{\int_{\lambda_{min}}^{\lambda_{max}=388\,nm} I(\lambda)d\lambda}{\int_{\lambda_{min}}^{\lambda_{max}=469\,nm} I(\lambda)d\lambda} \quad (A1.4)$$

As a result, it is possible to establish that for the case of the present study γ has a value of 0.92.

Appendix B.

The calculation of the *PTEF* requires the evaluation of the enthalpy of formation of *OH•* radicals. Serrano and de Lasa [16] have reported the assessment of this enthalpy for the case of photocatalytic treatment in water. A similar calculation process can be used in photocatalytic air treatment reactors.

The heterogeneous photocatalytic process involve photons of light (from the sunlight or an artificial source) exciting the TiO_2 and promoting electrons from the valence band to the conduction band of the semiconductor generating electron/hole pairs [40–42],

$$TiO_2 + h\nu \rightarrow h^+ + e^- \quad (A2.1)$$

The electron/holes pairs react with water molecules or hydroxyl ions that are adsorbed on the surface of TiO_2 producing hydroxyl radicals as follows

$$H_2O_{ads} \rightarrow OH^-_{ads} + H^+ \quad (A2.2)$$

$$OH^-_{ads} + h^+ \rightarrow OH_{ads}^{\bullet} \quad (A2.3)$$

At the same time, the formed electrons react with oxygen forming superoxide radicals, with hydrogen peroxide being formed according to Eqs. (A2.4)–(A2.7),

$$O_{2\,ads} + e^- \rightarrow O^{-\bullet}_{2\,ads} \quad (A2.4)$$

$$O^{-\bullet}_{2\,ads} + H^+ \rightarrow HO^{\bullet}_{2\,ads} \quad (A2.5)$$

$$O^{-\bullet}_{2\,ads} + HO^{\bullet}_{2\,ads} \rightarrow HO^-_{2\,ads} + O_{2\,ads} \quad (A2.6)$$

$$HO^-_{2\,ads} + H^+ \rightarrow H_2O_{2\,ads} \quad (A2.7)$$

One can multiply Eqs. (A2.2)–(A2.4) by a factor of 2 and following this, add the resulting equations to (A2.5)–(A2.7). This algebraic combination yields,

$$O_{2\,ads} + 2H_2O_{ads} + 2h\nu \rightarrow H_2O_{2\,ads} + 2OH_{ads}^{\bullet} \quad (A2.8)$$

Furthermore, there is also the possible conversion of hydrogen peroxide giving two extra hydroxyl radicals ($OH^{\bullet}$) via the following two steps,

$$H_2O_{2\,ads} + e^- \rightarrow OH_{ads}^{\bullet} + OH^-_{ads} \quad (A2.9)$$

$$OH^-_{ads} + h^+ \rightarrow OH^{\bullet}_{ads} \quad (A2.10)$$

Adding Eqs. (A2.9) and (A2.10) it yields,

$$H_2O_{2\,ads} + h\nu \rightarrow 2OH_{ads}^{\bullet} \quad (A2.11)$$

Summation of Eqs. (A2.8) and (A2.11) leads to the overall stoichiometric expression,

$$2H_2O_{(g)} + O_{2(g)} + 3h\nu \rightarrow 4OH_{ads}^{\bullet} \quad (A2.12)$$

Eq. (A2.12) shows that the overall stoichiometry for the formation of $OH^{\bullet}$ radicals can be described with 3 photons yielding 4 $OH^{\bullet}$. As a result, 133% is in principle the best quantum yield that one can obtain assuming that there is no photon-site recombination.

References

[1] M. Kaneko, I. Okura (Eds.), Photocatalysis: Science and Technology, Kodansha Springer, Tokyo/Berlin/New York, 2002.
[2] H. de Lasa, B. Serrano, M. Salaices, Photocatalytic Reaction Engineering, first ed., Springer, New York, 2005.
[3] Y. Paz, Photocatalytic treatment of air: from basic aspects to reactors, in: H.I. de Lasa, B. Serrano (Eds.), Adv. Chem. Eng., 36, 2009, pp. 289–336.
[4] J. Disdier, P. Pichat, D. Mas, Measuring the effect of photocatalytic purifiers on indoor air hydrocarbons and carbonyl pollutants, J. Air Waste Manage. Assoc. 55 (2005) 88–96.
[5] A. Mills, R.H. Davies, D. Worsley, Water purification by semiconductor photocatalysis, Chem. Soc. Rev. 22 (1993) 417–425.
[6] M. Trillas, M. Pujol, X. Domenech, Phenol photodegradation over titanium dioxide, J. Chem. Technol. Biotechnol. 55 (1992) 85–90.
[7] J. Taranto, D. Frochot, P. Pichat, Photocatalytic treatment of air: comparison of various TiO_2, coating methods, and supports using methanol or n-octane as test pollutant, Ind. Eng. Chem. Res. 48 (2009) 6229–6236.
[8] M.O. Alfano, M.I. Cabrera, A.E. Cassano, Photocatalytic reactions involving hydroxyl radical attack I. Reaction kinetics formulation with explicit photon absorption effects, J. Catal. 172 (1997) 370–379.
[9] J. Peral, X. Domènech, D.F. Ollis, Heterogeneous photocatalysis for purification, decontamination and deodorization of air, J. Chem. Technol. Biotechnol. 70 (1997) 117–140.
[10] F. Thevenet, O. Guaitella, E. Puzenat, C. Guillard, A. Rousseau, Influence of water vapour on plasma/photocatalytic oxidation efficiency of acetylene, Appl. Catal. B 84 (2008) 813–820.
[11] H. Ibrahim, H. de Lasa, Kinetic modeling of the photocatalytic degradation of air-borne pollutants, AIChE J. 50 (2004) 1017–1027.
[12] J. Cerdá, J.L. Marchetti, A.E. Cassano, Radiation efficiencies in elliptical photoreactors, Lat. Am. J. Heat Mass Transf. 1 (1977) 33–63.
[13] N. Serpone, A.V. Emeline, Suggested terms and definitions in photocatalysis and radiocatalysis, Int. J. Photoenergy 4 (2002) 91–131.
[14] H. Ibrahim, H. de Lasa, Photo-catalytic degradation of air borne pollutants. Apparent quantum efficiencies in a novel Photo-CREC-Air reactor, Chem. Eng. Sci. 58 (2003) 943–949.
[15] H. Ibrahim, Photo-catalytic reactor for the degradation of airborne pollutants: photo-conversion efficiency and kinetic modeling. Ph. D. Dissertation, The University of Western Ontario, London, Canada, 2001.
[16] B. Serrano, H. de Lasa, Photocatalytic degradation of water organic pollutants. Kinetic modeling and energy efficiency, Ind. Eng. Chem. Res. 36 (1997) 4705–4711.
[17] B. Serrano, A. Ortiz, J. Moreira, H. de Lasa, Energy efficiency in photocatalytic reactors for the full span of reactions times, Ind. Eng. Chem. Res. 48 (2009) 9864–9876.
[18] B. Serrano, M. Salaices, A. Ortiz, H. de Lasa, Quasi-equilibrium and non-equilibrium adsorption in heterogeneous photocatalysis, Chem. Eng. Sci. 62 (2007) 5160–5166.
[19] B. Ruscic, A.F. Wagner, L.B. Harding, R.L. Asher, D. Feller, D.A. Dixon, K. Peterson, Y. Song, X. Qian, C.Y. Ng, J. Liu, W. Chen, D.W. Schwenke, On the enthalpy of formation of hydroxyl radical and gas-phase bond dissociation energies of water and hydroxyl, J. Phys. Chem. A 106 (2002) 2727–2747.
[20] E. Sicilia, F.P. Di Maio, N. Russo, Heats of formation of oxygen-containing radicals from local spin density computations, J. Phys. Chem. 97 (1993) 528–530.
[21] D.D. Wagman, W.H. Evans, V.B. Parker, R.H. Schumm, I. Halow, S.M. Bailey, K.L. Churney, R.L. Nutall, The NBS Tables of chemical thermodynamic properties: selected values for inorganic and C1 and C2 organic substances in SI units, J. Phys. Chem. Ref. Data 11 (1982) 1.
[22] B.G. Kyle, Chemical and Process Thermodynamics, second ed., Prentice Hall, New York, 1992.
[23] H. Ibrahim, H. de Lasa, Photo-catalytic conversion of air borne pollutants. Effect of catalyst loading in a novel Photo-CREC-Air unit, Appl. Catal. B 38 (2002) 201–213.
[24] J. Peral, D. Ollis, Heterogenous photocatalytic oxidation of gas-phase organics for air purification: acetone, 1-butanol, butyraldehyde, formaldehyde and m-xylene oxidation, J. Catal. 36 (1992) 554–565.
[25] N. Negishi, S. Matsuzawa, K. Takeuchi, P. Pichat, Transparent micrometer-thick TiO_2 films on SiO_2-coated glass prepared by repeated dip-coating/calcination: characteristics and photocatalytic activities for removing acetaldehyde or toluene in air, Chem. Mater. 19 (2007) 3808–3814.
[26] S. Romero-Vargas Castrillón, H. Ibrahim, H. de Lasa, Flowfield investigation in a photocatalytic reactor for air treatment (photo-CREC–air), Chem. Eng. Sci. 61 (2006) 3343–3361.
[27] C.P. Chang, J.N. Chen, M.C. Lu, Heterogeneous photocatalytic oxidation of acetone for air purification by near UV-irradiated titanium dioxide, J. Environ. Sci. Health Toxic/Hazard Subst. Environ. Eng. (2003) 1131–1143.
[28] W. Choi, J.Y. Ko, H. Park, J.S. Chung, Investigation on TiO_2-coated optical fibers for gas-phase photocatalytic oxidation of acetone, Appl. Catal. B 31 (2001) 209–220.
[29] J.M. Coronado, S. Kataoka, I. Tejedor-Tejedor, M.A. Abderson, Dynamic phenomena during the photocatalytic oxidation of ethanol and acetone over nanocrystalline TiO_2: simultaneous FTIR analysis of gas and surface species, J. Catal. 219 (2003) 219–230.
[30] M.D. Hernández-Alonso, I. Tejedor-Tejedor, J.M. Coronado, M.C. Anderson, J. Soria, Operando FTIR study of the photocatalytic oxidation of acetone in air over TiO_2-ZrO_2 thin films, Catal. Today 143 (2009) 364–373.
[31] H. Kim, W. Choi, Effects of surface fluorination of TiO_2 on photocatalytic oxidation of gaseous acetaldehyde, Appl. Catal. B 69 (2007) 127–132.
[32] I. Sopyan, Kinetic analysis on photocatalytic degradation of gaseous acetaldehyde, ammonia and hydrogen sulfide on nanosized porous TiO_2 films, Sci. Technol. Adv. Mater. 8 (2007) 33–39.
[33] T. Arai, M. Yanagida, Y. Konishi, Y. Iwasaki, H. Sugihara, K. Sayama, Promotion effect of CuO co-catalyst on WO_3-catalized photodegradation of organic substances, Catal. Commun. 9 (2008) 1254–1258.
[34] A.S. Besov, A.V. Vorontsov, Acceleration of acetone destruction process under synergistic action of photocatalytic oxidation and barrier discharge, Plasma Chem. Plasma Process. 27 (2007) 624–634.
[35] T. Morikawa, Y. Irokawa, T. Ohwaki, Enhanced photocatalytic activity of TiO_2–xNx loaded with cooper ions under visible light irradiation, Appl. Catal. A 314 (2006) 123–127.
[36] C.M. Schmidt, A.M. Buchbinder, E. Weitz, F.M. Geiger, Photochemistry of the indoor air pollutant acetone on Degussa P25 TiO_2 studied by chemical ionization mass spectrometry, J. Phys. Chem. A 111 (2007) 13023–13031.
[37] A. Cassano, C. Martín, R. Brandi, O. Alfano, Photoreactor analysis and design: fundamentals and applications, Ind. Eng. Chem. Res. 34 (1995) 2155–2201.
[38] M.R. Nimlos, E.J. Wolfrum, M.L. Brewer, J.A. Fennell, G. Bintner, Gas-phase heterogeneous oxidation of ethanol: pathways and kinetic modeling, Environ. Sci. Technol. 30 (1996) 3102–3110.
[39] G.B. Raupp, C.T. Junio, Photocatalytic oxidation of oxygenated air toxics, Appl. Surf. Sci. 72 (1993) 321–327.
[40] K. Okamoto, Y. Yasunori, T. Hirok, T. Masashi, T. Akira, Heterogeneous photocatalytic decomposition of phenol over TiO_2 powder, Bull. Chem. Soc. Jpn. 58 (1985) 2015–2022.
[41] M.A. Fox, M.T. Dulay, Heterogeneous photocatalysis, Chem. Rev. 93 (1993) 341–350.
[42] M.R. Hoffmann, S.T. Martin, W. Choi, Environmental applications of semiconductor photocatalysis, Chem. Rev. 95 (1995) 69–77.